JOURNAL OF SYNCHROTRON RADIATION
ISSN 1600-5775

XMCD studies of magnetic polarization at Mo atoms in CoMo alloy and magnetically coupled Co/Mo multilayers

Andrzej Wawro,[a]* Ewelina Milińska,[a] Zbigniew Kurant,[b] Aleksiej Pietruczik,[a] Jarosław Kanak,[c] Katharina Ollefs,[d] Fabrice Wilhelm,[d] Andrei Rogalev[d] and Andrzej Maziewski[b]

[a]Institute of Physics, Polish Academy of Sciences, Aleja Lotnikow 32/46, Warsaw PL-02668, Poland, [b]Department of Physics, University of Białystok, ul. Ciołkowskiego 1L, Białystok 15-245, Poland, [c]Department of Electronics, AGH University of Science and Technology, Al. Mickiewicza 30, Kraków 30-059, Poland, and [d]European Synchrotron Radiation Facility (ESRF), 71 Avenue des Martyrs, 38043 Grenoble Cedex 9, France.
*Correspondence e-mail: wawro@ifpan.edu.pl

Received 30 November 2017
Accepted 8 June 2018

Edited by V. Favre-Nicolin, CEA and Université Joseph Fourier, France

Keywords: interlayer magnetic coupling; induced magnetic moment; magnetic multilayers; X-ray magnetic circular dichroism.

Magnetic polarization of Mo atoms in $Co_{96}Mo_4$ alloy film and Co/Mo multilayered structures has been studied by X-ray magnetic circular dichroism. Samples with Mo spacers of two different thicknesses (0.9 nm and 1.8 nm) were investigated. Mo atoms receive a magnetic moment of $-0.21\mu_B$ in the alloy. In the multilayer with the thinner Mo spacer (d_{Mo} = 0.9 nm) the magnetic moment is much smaller ($-0.03\mu_B$). In both cases the measured induced moment at the Mo site is oriented antiparallel to the moment at the Co atoms. The presence of the induced moment in the Mo spacer coincides with antiferromagnetic coupling between the Co component slabs. In contrast, neither measurable induced moment at the Mo site nor interlayer coupling between the Co layers has been found for the multilayer with the thicker Mo spacer. Possible mechanisms of the coupling associated with the induced moment are discussed in detail.

1. Introduction

Artificially fabricated materials such as multilayers or patterned structures, confined to the nanometre scale at least in one dimension, display novel properties that are different from the bulk. Among them are magnetic multilayers with properties determined by a significant fraction of atoms located at the interfaces or layer thicknesses smaller than the characteristic lengths (*e.g.* electron mean free path or spin diffusion length) (Hellman *et al.*, 2017; Sander *et al.*, 2017). Interlayer magnetic coupling has been one of the most intensively studied phenomena during the last three decades (Grünberg *et al.*, 1986; Carbone & Alvarado, 1987; Grolier *et al.*, 1993). Its oscillating character is frequently explained by the Ruderman–Kittel–Kasuya–Yosida (RKKY) interaction mediated by the electrons, the model initially developed for diluted magnetic ions (Ruderman & Kittel, 1954; Kasuya, 1956; Yosida, 1957). The functionality increase requirement of such structures needs further modifications to obtain the desired properties. Such effects have been achieved by fabrication methods (Schlage *et al.*, 2016), appropriate configuration of the grown structures (Bandiera *et al.*, 2012; Hellwig *et al.*, 2003; Fallarino *et al.*, 2016; Stobiecki *et al.*, 2008; Hsu *et al.*, 2015; Gareev *et al.*, 2011; Saerbeck *et al.*, 2011) and post-growth treatment (Wawro *et al.*, 2017*a*; Demokritov *et al.*, 2003; Demidov *et al.*, 2004; McCord *et al.*, 2011; Greene *et al.*, 2014; Bali *et al.*, 2014).

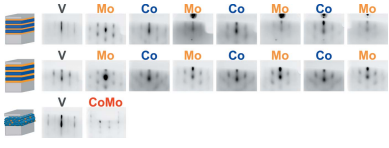

© 2018 International Union of Crystallography

An understanding of physical mechanisms responsible for unique features is fundamental in material design with desired properties. In magnetic multilayers an interface magnetism, affected by the local structural and electronic modifications at the border between the component materials, frequently plays a crucial role. Non-magnetic atoms in the bulk may possess a magnetic moment upon proximity interactions. Such sophisticated effects can be successfully probed by X-ray magnetic circular dichroism (XMCD). Predominantly, 4*d* and 5*d* metals such as Mo or W, non-magnetic in bulk, are the focus of our attention. However, the contribution of Mo to the interface magnetism has not been studied deeply yet. So far, induced magnetic moments at the Mo site have been studied mainly in alloys or complex compounds.

Sr_2FeMoO_6 has been intensively studied for spintronic applications because it displays the total spin polarization of charge carriers due to a gap occurrence in one spin channel. The observed properties are explained by the configuration of five localized *d* electrons resulting in a high spin state of the Fe site and *s* electron shared between Mo and the other sites (Besse *et al.*, 2002). A spin magnetic moment of $3.05\mu_B$ deduced from XMCD measurements at Fe and an induced one ($-0.32\mu_B$) at Mo are coupled antiparallel giving rise to ferrimagnetic ordering. Experimental observations were confirmed by *ab initio* calculations carried out for the Mo $L_{2,3}$-edges (Kanchana *et al.*, 2007). The spin moment and orbital moment at the Mo site equal to $-0.29\mu_B$ and $0.020\mu_B$, respectively, are antiparallel in accordance with Hund's third rule. In pyrochlore-type molibdenates $R_2Mo_2O_7$ (where *R* is a rare-earth element) a correlation of the induced moment at Mo has been investigated depending on the element *R*. A moment at the Mo site as high as $1.54\mu_B$ was found for Sm (Imada *et al.*, 2005). In copper octacyanomolibdemate the observed photo-induced magnetism, reversible after heating at 300 K, was attributed to the spin conversion between the low- and high-spin Mo(IV) ions. XMCD measurements show that the average moment induced at the Mo ion is equal to $0.42\mu_B$. This value corresponds to a third of the Mo ions which have been photo-transformed upon laser irradiation (Brossard *et al.*, 2012). A higher moment (orbital $0.13\mu_B$ and spin $1.22\mu_B$) induced in the metastable state of the high-spin triplet Mo(IV) was reported by Arrio *et al.* (2010). Due to a strong hybridization of the O 2*p*–Mo 4*d* orbitals a ferromagnetic coupling was observed in MoO_2 (Thakur *et al.*, 2009).

The magnetic moment induced in *d*-band elements, forming interfaces, has also been investigated in multilayered metallic structures. A considerable magnetic moment of about $0.2\mu_B$ was probed by XMCD in the non-magnetic 5*d* spacers W and Ir separating Fe thin films in multilayered structures (Wilhelm *et al.*, 2001). Tungsten was found to be coupled antiferromagnetically and Ir ferromagnetically to adjacent Fe layers. In particular, in a less than half-filled 5*d* shell in W the spin and orbital magnetic moments were coupled in parallel, contrary to expectations governed by Hund's third rule. An antiparallel alignment of induced magnetic moments across the W spacer was found in the Fe/W multilayer (Jaouen *et al.*, 2004). A magnetic moment of $0.4\mu_B$ at the W site in the first atomic layer was antiparallel to the Fe magnetic moment, similar to observations reported in the previously cited work (Wilhelm *et al.*, 2001). A moment in the next W atomic layer was lower and antiparallel to that forming the interface. Deeper insight into W spacers revealed a damped oscillation similar to the RKKY interactions. The measured moments at the W sites were considerably larger than those predicted by theoretical calculations. Such a moment increase can be associated with the higher Fe coordination around W atoms due to interface roughness, as confirmed by the numerical calculations (Tyer *et al.*, 2003). The XMCD spectra recorded for Mo atoms at the *L* and *M* absorption edges were compared in terms of signal quality dependent on the circular polarization contribution to the total beam and a signal-to-background ratio in the Fe/Mo multilayers (Tomaz *et al.*, 1998). The *M* absorption edge was deduced as preferred for Mo element. The estimated induced magnetic moment was as high as $0.4\mu_B$. The magnetic moment at the Mo site was found to be antiparallel aligned to the moment of the Fe layers.

In this work we study the magnetic polarization at the Mo atoms of a non-magnetic (in bulk) spacer in Co/Mo multilayers. Magnetization of the Co layers separated by an Mo spacer is aligned antiparallel (Wawro *et al.*, 2017*a*) merely in the narrow range of the Mo spacer thickness around 0.9 nm. To explore the role of induced moment at the Mo spacer atoms in the interlayer coupling, two types of Co/Mo multilayers, with antiparallel coupling and without coupling, are studied by XMCD. Also, a $Co_{96}Mo_4$ alloy with Mo atoms diluted in the Co matrix is investigated. It is expected that in such a reference structure the induced magnetic moment at the Mo atoms takes its maximum value. Various possible mechanisms responsible for the observed interlayer coupling, including the induced magnetic moment at the Mo spacer atoms, are discussed in detail.

2. Experimental details

The investigated samples were grown in a molecular beam epitaxy (MBE) system in the following configuration: S/V/$[Mo(d_{Mo})/Co(4\ nm)]_3/Mo(d_{Mo})$/V, where S denotes a sapphire (11–20) substrate. Vanadium buffer, 20 nm thick, was deposited onto substrate at 600°C to reduce surface corrugation. Such a buffer type offers good conditions for epitaxial growth for the layered samples. Moreover, V buffer was chosen to avoid an overlap in photon energy with the absorption edges of Mo and Co. Sequentially grown Mo and Co layers as well as a V overlayer, 5 nm thick, were deposited at room temperature. During the deposition procedure the crystalline structure of the grown samples was monitored by 12 keV reflection high-energy electron diffraction (RHEED). Two layered samples with d_{Co} = 4 nm and various Mo spacer thicknesses d_{Mo} = 0.9 nm and d_{Mo} = 1.8 nm, exhibiting antiparallel and parallel in-plane alignments of the Co layer magnetization, respectively, were prepared. The third investigated sample, S/V/$Co_{96}Mo_4$/V, containing an alloy film, 110 nm thick, was fabricated by co-evaporation of Co and Mo at the V buffer kept at room temperature. Selected composition of the alloy

was obtained by appropriate setting of the evaporation rates of each element. For this composition, every Mo atom is statistically fully coordinated by the Co atoms.

The crystalline structure of the samples and interface quality of the layered systems were investigated by high-angle X-ray diffraction (XRD), θ–2θ geometry, with a step of 0.04° and X-ray reflectivity (XRR) with a step of 0.004°. The measurements were performed using an X'Pert-MPD diffractometer with a Cu anode and graphite monochromator.

The magnetic properties were probed using a magnetometer exploiting the magnetooptical Kerr effect. Because the magnetization of the studied samples was aligned in the plane, the measurements were performed in a longitudinal configuration (LMOKE).

The XMCD experiments at the Mo $L_{2,3}$-edges were carried out at room temperature at the ESRF beamline ID12, which is dedicated to polarization-dependent X-ray absorption experiments. A helical undulator, Helios-II, emitting the first harmonic in the energy range 2–6 keV was a source of circular-polarized X-rays. The high (97%) circular polarization rate of the undulator radiation dropped to about 12% at the Mo L_3-edge (2523 eV) and 4% at the Mo L_2-edge (2629 eV) after passing through the double-crystal Si(111) monochromator, because the Bragg angle of the monochromator was close to the Brewster angle at these photon energies. The samples were mounted in a small vacuum-chamber inserted between the poles of an electromagnet providing a magnetic field up to 0.9 T. The angle between incoming X-rays, which were parallel to the magnetic field and the sample surface, was set to 10°. X-ray absorption near-edge structure (XANES) spectra were recorded using total fluorescence yield detection mode with a Si photodiode mounted inside the vacuum chamber at an angle of 90° to the incident X-ray beam. This detection technique probes the whole volume of the layered Co/Mo structure (approximately 20 nm thick). The XMCD signal was obtained by flipping the direction of the magnetic field at every photon energy of the XANES spectrum. In order to ensure that the XMCD results were free of artefacts, the signal was also recorded after reversing the helicity of the X-ray beam. Due to the small film thickness, self-absorption effects have not been checked.

3. Results

The structure of every completed component layer in the multilayers and of the alloy film was checked by RHEED. The sequences of patterns are shown in Fig. 1. Characteristic streaks prove that the multilayered structures are epitaxial. The streak quality of the same layer type is similar regardless of the growth stage. This means that the structure and properties of the consecutive component layers are reproducible and do not alter with the in-depth position in the system. The streaks from the Co layer are more continuous than from Mo. This may suggest that the surface roughness of the Mo component layers is higher than that of Co. The transmission electron microscopy image of the sample with a similar structure, grown under the same conditions, but with higher

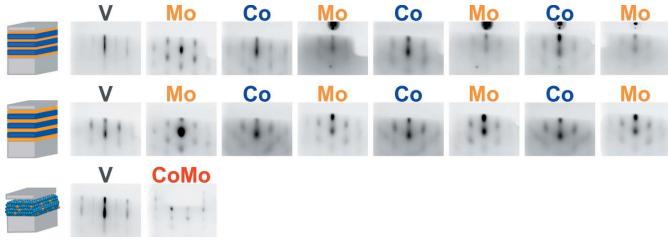

Figure 1
Sequences of the RHEED patterns recorded after completion of each component layer (upper row: sample with the thinner Mo spacer; middle row: sample with the thicker Mo spacer; bottom row: alloy layer at the final stage of the deposition process).

bilayer repetition number (not presented in this work), shows that the component layers are sharp and continuous. Also, the XANES profile at the Co K-edge typical of a hexagonal close-packed (h.c.p.) structure (Wawro *et al.*, 2017*b*) proves that Co grows in the bulk-like mode and alloying at the interfaces is negligible. Slightly dotted RHEED streaks from the alloy show that the crystalline structure is also maintained; however, the surface is much rougher than that of the layered samples.

The internal structure of the samples has also been studied by high-angle XRD and XRR. Fig. 2 shows XRD θ–2θ profiles of the samples. The strong peaks from the sapphire substrate (around 38°), the buffer and cap V layers (around 42.5°) are common features in the shown spectra. In the layered samples the signal from the Co layers is low due to their small thickness. It is visible as weak peaks broadening between 44° and 49°. Their width matches well to a value determined from the Scherrer equation for a particle size equal to the Co layer thickness. In the spectra from the layered structures, the fine oscillations, so-called thickness fringes, are very clear. They provide evidence of a smooth surface and, in consequence, interfaces in this type of sample. In the spectrum from the alloy sample, two stronger peaks from Co at 44.5° and 47° are very distinct. They are shifted from Co face-centred cubic

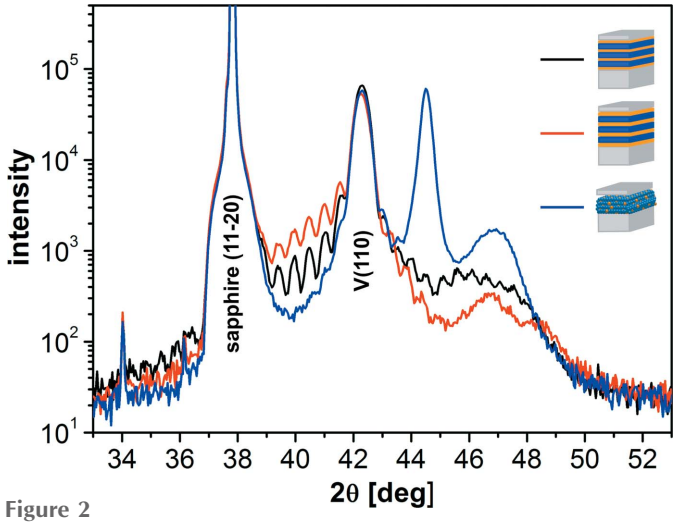

Figure 2
XRD θ–2θ profiles of the layered samples with d_{Mo} = 0.9 nm (black), d_{Mo} = 1.8 nm (red) and the alloy sample (blue).

(f.c.c.) (111) and Co h.c.p. (002) bulk positions. This may suggest that in the Co layer f.c.c. and h.c.p. structures coexist or peaks are shifted because Mo atoms deform the lattice of the Co matrix.

The measured XRR curves shown in Fig. 3 depict clear differences between the layered samples and thick alloy film. The Bragg peaks separated by two Kiessig fringes are typical of a layered structure with triple repetition of the bilayer. Different densities of the peaks result from various periodicities of the layered samples. The reflectivity curve from the thick alloy sample exhibits dense uniform fringes as expected for the thick sample. The signal intensity decreases more rapidly with angle due to the higher surface roughness in comparison with the layered samples. The numerically calculated curves fit excellently to the experimental lines. This procedure confirmed the assumed thicknesses of the component layers.

Investigated samples are magnetized in the plane. Fig. 4 depicts the dependence of the normalized magnetization remanence m_R on Mo spacer thickness (determined from the sample with the Mo wedge-shaped spacer, not discussed in this work) and two hysteresis LMOKE loops from the layered samples with d_{Mo} equal to 0.9 nm and 1.8 nm.

A dip plateau in m_R (d_{Mo}) around d_{Mo} = 0.9 nm is distinct (Fig. 4*a*). It corresponds to antiparallel magnetization coupling of the component Co layers. For the thinner and thicker d_{Mo}, m_R takes a value of 1, which shows that at remanence the magnetization of all Co layers is oriented in the same direction.

Three component sub-loops from the sample with d_{Mo} = 0.9 nm show the antiferromagnetic coupling of the Co slabs

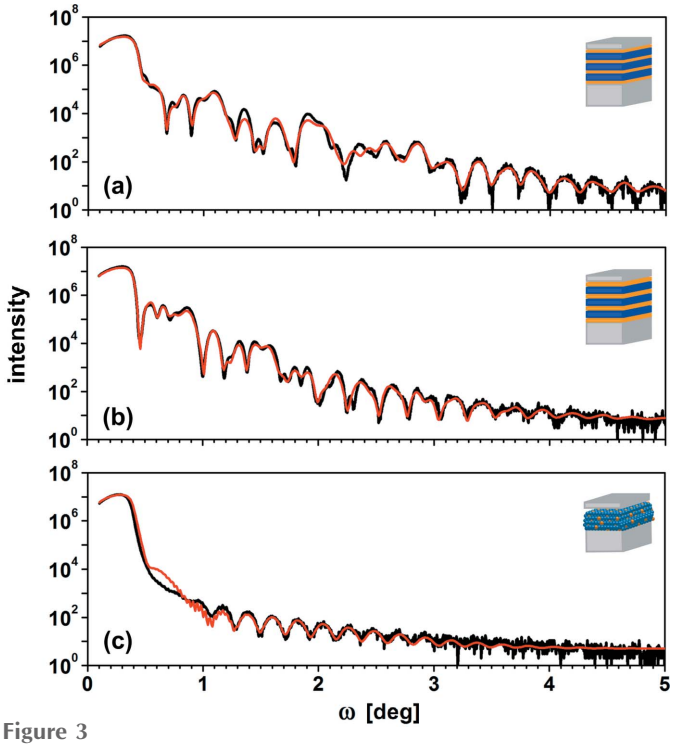

Figure 3
XRR curves (black lines) and numerical fittings (red lines) for the layered samples with (*a*) d_{Mo} = 0.9 nm, (*b*) d_{Mo} = 1.8 nm and (*c*) the alloy sample.

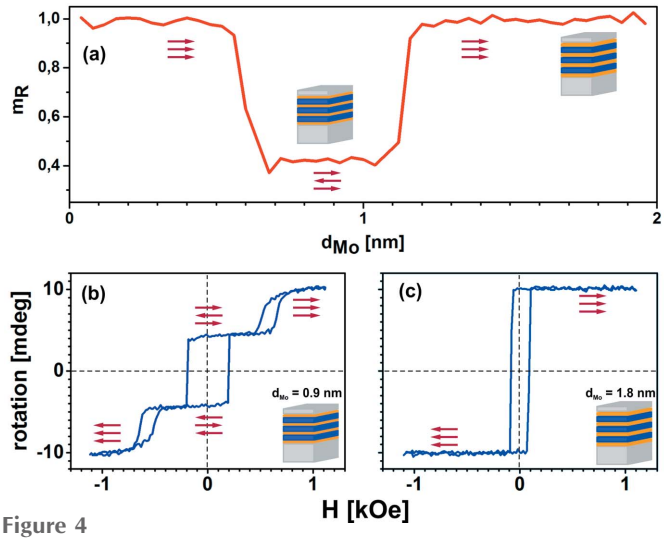

Figure 4
(*a*) Normalized magnetization at the remanent state as a function of the Mo spacer thickness. The positions of the layered samples with uniform thicknesses of the component layers at the d_{Mo} scale are also shown. LMOKE hysteresis loops for the sample exhibiting (*b*) antiparallel coupling (d_{Mo} = 0.9 nm) and (*c*) parallel alignment of magnetization (d_{Mo} = 1.8 nm). The arrows illustrate magnetization alignments in the component Co layers.

(Fig. 4*b*). In saturation the Co layers are magnetized along the applied magnetic field. A decrease in the field below 0.8 kOe results in the magnetization configuration change to the antiparallel alignment of the Co layers. Such a configuration is stable at remanence. Under a field applied in the opposite direction, the magnetization of the whole sample reverses by 180°, retaining the antiparallel coupling of the component Co layers. A further increase of the field aligns the magnetization of all the Co slabs in parallel, leading to sample saturation.

Magnetization reversal of the sample with the thicker Mo spacer (Fig. 4*c*) is less complicated. Magnetization of all Co layers is oriented in the same direction at saturation and at remanence. A perfectly rectangular shape of the loop proves that all the component Co layers undergo magnetization reversal simultaneously, which may suggest that magnetization of this sample is coupled in parallel.

XANES and XMCD spectra were measured at the Mo L_2- and L_3-edges both in the layered samples and in the alloy film (Fig. 5). The XMCD signal for the layered sample with the thicker Mo spacer was below the detection threshold (not shown), although the XANES signal was very distinct. The weak peak at energy ~10 eV above the edge is the fingerprint of a good crystalline quality of the Mo spacer (Evans & Mosselmans, 1991). Magnetic polarization of Mo 4*d* states is very clear. The same signs of the spectra recorded at the $L_{2,3}$-edges for the layered and alloy samples can be easily noticed.

In order to perform a quantitative analysis, the XANES spectra were normalized and the XMCD signal was corrected for the incomplete circular polarization rate. Before applying the sum rules the X-ray absorption cross section per hole was retrieved. For this purpose the XANES spectra for the L_3- and L_2-edges were normalized to 1 and to 1/2, respectively, according to the statistical branching ratio. The area under the

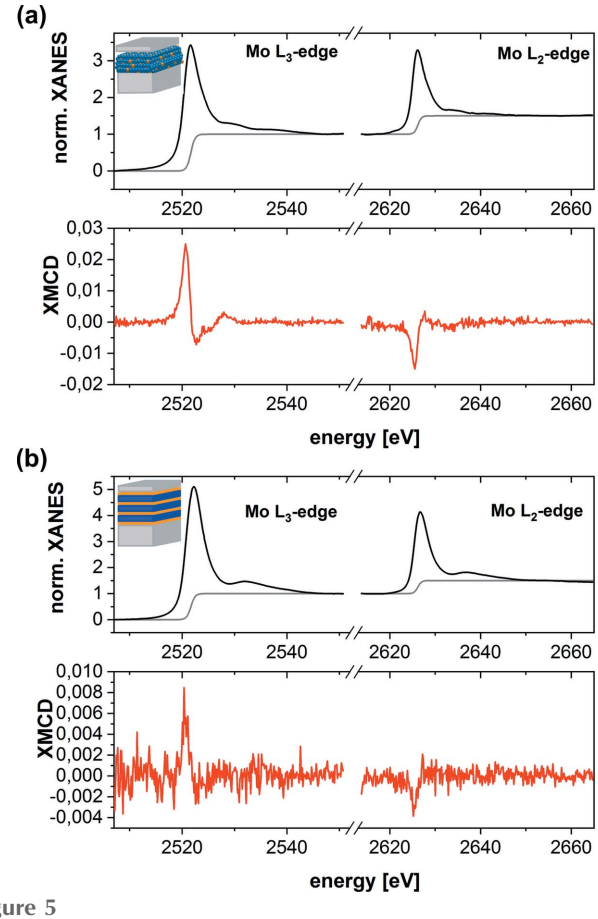

Figure 5
XANES (black lines) and XMCD (red lines) spectra from (*a*) the alloy sample and (*b*) the layered sample with d_{Mo} = 0.9 nm. Profiles of the step functions are plotted in grey.

L_3 and L_2 white lines is proportional to the number of holes in the 4*d* band of Mo. The transition to continuum states simulated by a step function was subtracted from the normalized XANES spectra. The value of this area was divided by the number of 4*d* holes, which was taken from band-structure calculations of Mo metal (Yaresko, 2016) and found to be equal to n_h = 5.46.

To determine the spin and orbital components of the magnetic moments induced at Mo atoms, the magneto-optical sum rules were applied (Thole *et al.*, 1992; Carra *et al.*, 1993). In calculation the formulas for m_S and m_l were used according to the work of Stöhr (1995) with the X-ray absorption cross section per hole determined previously $C = (I_{L2} + I_{L3})/n_h$. The orbital moment is given by the following sum rule: $m_l = 2\,\mu_B(A + B)/3C$, where A and B are the integrated areas of the L_3 and L_2 XMCD peaks, respectively. The second sum rule $(A - 2B) = -Cm_S/\mu_B$ yields the spin component m_S, under the assumption that there is no spin anisotropy in Mo, *i.e.* an expectation value of $T_Z = 0$, as the orbital moment is very low.

The derived moments from the XMCD spectra shown in Figs. 5(*a*) and 5(*b*) are the following: $m_S = -0.21\mu_B$ and $m_l = 0.014\mu_B$ for the alloy sample and $m_S = -0.03\mu_B$ and $m_l = 0.005\mu_B$ for the multilayered sample (d_{Mo} = 0.9 nm) (all determined parameters are listed in Table 1). Negative signs indicate that the moment is antiparallel to the applied magnetic field and therefore to the Co magnetization. The value of the magnetic moment in the CoMo alloy, comparable with the value found for localized systems (Brossard *et al.*, 2012), is twice smaller than the moment found for FeMo (Tomaz *et al.*, 1998). Taking into account the smaller spin moment of Co, compared with Fe, the deduced magnetic polarization found for Mo is reasonable. A very weak contribution of the orbital component to the measured signal is typical of delocalized systems. The coupling of the spin and orbital moments at the Mo atom is antiparallel. In the Mo atom, the *d* band is less than half-filled which invokes an antiparallel alignment of the spin and orbital moment, according to Hund's rule.

Table 1
Parameters determined from the XMCD sum rules (a detailed description is provided in the text).

Sample	*A*	*B*	m_S	m_l
Alloy $Co_{96}Mo_4$	−0.27	0.1	−0.21	0.014
Layered (d_{Mo} = 0.9 nm)	−0.042	0.0621	−0.03	0.005

4. Discussion

In this section we briefly review mechanisms that might be responsible for the antiparallel magnetization coupling of the Co layers. We discuss possible scenarios in the context of the induced magnetic moment at the atoms of the Mo spacer.

Numerous models based on indirect exchange interactions have been proposed to explain interlayer coupling across a non-magnetic spacer. One of them exploits the RKKY approach assuming an oscillating type of interaction, originally developed for localized magnetic moments. The coupling is mediated through conduction electrons (*s–d* or *s–f* exchange). Since in transition ferromagnetic metals (*e.g.* Co) 3*d* electron states are strongly hybridized, a description for delocalized electrons has been proposed (Lacroix & Gavigan, 1991; Bruno & Chappert, 1992). Observed coupling oscillations have been explained with the help of the sharp cut-offs in the momentum space at the Fermi surface in the spacer layer.

Another model was based on the observation that reflection of the electrons at the spacer/ferromagnet interface is spin-dependent. Spatial confinement of the electrons was analogous to the electron behaviour in the quantum well (QW) (Hathaway & Cullen, 1992; Barnaś, 1992; Edwards *et al.*, 1991). The states in the QW evolve with the change of the spacer layer thickness. When the QW level crosses the Fermi surface the energy of the multilayer increases. To lower the energy of the system the magnetization switches from a parallel to an antiparallel alignment.

Both approaches described above yield the same oscillatory and decaying character of the interaction. They are also well applicable for prefect structures with smooth and sharp interfaces.

In more realistic multilayer structures the interfaces are less perfect and display roughness. In some cases the roughness

can be modelled as the spatially fluctuating thickness of the spacer. Due to interlayer exchange coupling, the magnetization in the ferromagnetic layers does not rotate rapidly in space. Instead, an orthogonal orientation of the magnetization occurs as predicted theoretically by Slonczewski (1991, 1995), who introduced a biquadratic contribution to the coupling, shown experimentally by Demokritov *et al.* (1994). Such magnetic alignment was not observed in our samples.

Magnetic poles appearing at the interface are another consequence of the roughness. The poles exist because direct exchange interactions in the ferromagnetic layer prevents spin rotation from following the wavy profile of the interface. If the spacer thickness is relatively low the poles may lead to magnetostatic coupling between the ferromagnetic component layers. When the roughness is in phase, *i.e.* the next interface reproduces the previous one, then the magnetic layers are coupled in parallel (called orange peel coupling, as proposed by Neel) (Schrag *et al.*, 2000; Chopra *et al.*, 2000). In the case of uncorrelated roughness a contribution from the mentioned orange peel coupling is suppressed.

The above discussed mechanisms cannot explain unequivocally the antiparallel coupling observed in the Co/Mo multilayers. Due to the interface roughness the mechanisms involving RKKY interactions or QW behaviour in pure form may not be entirely appropriate. The contribution of correlated roughness seems to be not substantial as the antiparallel alignment of magnetization is well developed. One may also rule out a pin-hole coupling effect which might result from the roughness. Bridging should give rise to a local direct exchange between the Co layers manifesting in parallel alignment. Despite the roughness a biquadratic coupling is not present in this d_{Mo} thickness range. Due to lack of convincing explanation based on the above mechanisms the role of the induced magnetic moments at Mo spacer atoms should be taken into consideration.

The induced moment obtained from XMCD measurements at the Mo site in the alloy sample serves as a reference signal. In this sample every Mo atom is fully coordinated by the atoms of the Co matrix. Moreover, every two Mo atoms should be separated statistically by two Co atoms located between them. Therefore, it is expected that in the alloy sample the induced magnetic moment reaches a maximum possible value.

In the layered sample with d_{Mo} = 0.9 nm the magnetic moment is smaller by almost an order of magnitude in comparison with the alloy sample and has not been detected in the sample with d_{Mo} = 1.8 nm. The pure XMCD signal originates merely from the Mo atoms with induced moment. The suppression of the induced moment may be partially explained by the lower coordination of Mo atoms in the layered samples. However, the roughness of the interfaces should rather enhance the moment at the Mo site in comparison with ideally flat interfaces (Tyer *et al.*, 2003).

In the first possible interpretation the magnetic moment is induced only at the Mo atomic layer forming the interface with the Co layer. When the Mo spacer is thicker, the XMCD signal becomes lower with respect to the intensity of the distinct white line. Above a certain thickness threshold it may become comparable with the noise level and therefore undetectable, as observed in the sample with d_{Mo} = 1.8 nm.

However, the interlayer coupling strength in the multilayer with d_{Mo} = 0.9 nm is rather large whereas the measured giant magnetoresistance (GMR) is very low. In the layered system composed of five Co layers coupled antiparallel, the GMR signal reaches a level of 0.1% (transport measurements are not the subject of this work and will be discussed elsewhere). At the Mo(110)/Co(0001) interface both a structural mismatch (body-centred cubic *versus* close-packed) and a lattice parameter discrepancy take place. Moreover, rapid relaxation of the Co lattice grown at the Mo buffer suggests high density of dislocations (Wawro *et al.*, 2017*b*). These factors may cause a substantial scattering of the electrons and their spins. If only the RKKY mechanism is responsible for the observed strong interlayer coupling it should be effective merely in the interface regions of the Co layers. In such a case the central part of the Co layer would play a shunting role, and therefore substantially lower the GMR, as observed experimentally.

In the second interpretation, coinciding with the strong coupling and very weak GMR, the substantial suppression of the XMCD signal in the layered sample with the thinner Mo spacer may be caused by the antiparallel alignment of the relatively strong moments in the sequential atomic layers of the Mo spacer, similarly to the Fe/W system (Jaouen *et al.*, 2004). Such a spin configuration is schematically illustrated in Fig. 6(*a*). At the smaller and larger Mo spacer thicknesses, the magnetization of the component Co layers is oriented in the same direction (Fig. 4*a*). Antiparallel coupling of the Co layer magnetization occurs only in the narrow d_{Mo} range corresponding to the four Mo atomic layers. The combination of antiparallel coupling between the Co and Mo moments at the interface and between the consecutive Mo layers, by analogy to the Fe/W system (Figs. 6*b* and 6*c*), explains this interlayer coupling well, suggesting its exchange character. Following such an explanation, the antiparallel interlayer coupling should be expected when d_{Mo} corresponds to even numbers of atomic monolayers in the Mo spacer. Most probably the two-monolayer-thick spacer is not continuous, and the coupling is governed by the ferromagnetic bridges (pinholes). In the case

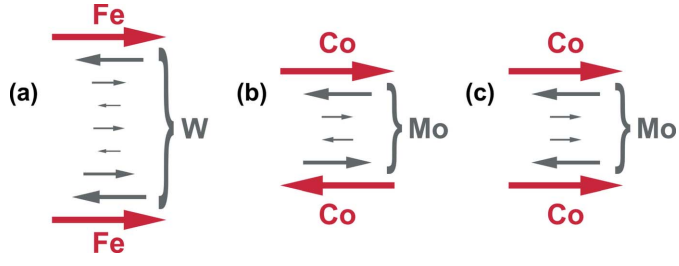

Figure 6
Schematic representation of the induced magnetic moment (grey arrows) alignment in individual atomic layers (*a*) across the W spacer thickness in Fe/W structures (Jaouen *et al.*, 2004), and across the Mo spacer (*b*) without magnetic field, and in the sample saturating field (*c*) during XMCD measurements. Red arrows illustrate magnetization alignment of magnetic layers: (*a*) Fe in Fe/W multilayers and (*b*, *c*) Co in Co/Mo studied structures.

of six and more monolayers the induced moments in the central part of the Mo spacer are too small to force the antiparallel coupling of the whole system through the exchange interactions.

5. Conclusions

Strongly antiparallel coupled magnetization of the Co films in Co/Mo multilayers can be explained in the frame of two models. In the first possibility the RKKY mechanism is responsible for the coupling. Then magnetic moments at the atoms of the Mo spacers may be induced merely in the atomic layers at the interface. However, the low value of the magnetoresistance with reference to the coupling strength suggests that the interlayer coupling, mediated by itinerant electrons, is confined only to the outer parts of the Co layers forming the interfaces. In the second approach, the antiparallel interlayer coupling can be explained in terms of the exchange interactions expanding across the spacer. Antiparallel alignment of magnetic moments induced in the consecutive Mo atomic layers as well as with the Co layers at the interfaces explains reasonably the strong interlayer coupling between the Co films in the narrow range of the Mo spacer thickness. Because we cannot prove unequivocally which type of interaction is dominant, we believe that our work will be an inspiration for further research.

Funding information

The following funding is acknowledged: National Science Centre in Poland (grant No. 2014/13/B/ST5/01834).

References

Arrio, M. A., Long, J., Cartier dit Moulin, Ch., Bachschmidt, A., Marvaud, V., Rogalev, A., Mathonière, C., Wilhelm, F. & Sainctavit, P. (2010). *J. Phys. Chem. C*, **114**, 593–600.

Bali, R., Wintz, S., Meutzner, F., Hübner, R., Boucher, R., Ünal, A. A., Valencia, S., Neudert, A., Potzger, K., Bauch, J., Kronast, F., Facsko, S., Lindner, J. & Fassbender, J. (2014). *Nano Lett.* **14**, 435–441.

Bandiera, S., Sousa, R. C., Rodmacq, B. & Dieny, B. (2012). *Appl. Phys. Lett.* **100**, 142410.

Barnaś, J. (1992). *J. Magn. Magn. Mater.* **111**, L215–L219.

Besse, M., Cros, V., Barthélémy, A., Jaffrès, H., Vogel, J., Petroff, F., Mirone, A., Tagliaferri, A., Bencok, P., Decorse, P., Berthet, P., Szotek, Z., Temmerman, W. M., Dhesi, S. S., Brookes, N. B., Rogalev, A. & Fert, A. (2002). *Europhys. Lett.* **60**, 608–614.

Brossard, S., Volatron, F., Lisnard, L., Arrio, M. A., Catala, L., Mathonière, C., Mallah, T., Cartier dit Moulin, Ch., Rogalev, A., Wilhelm, F., Smekhova, A. & Sainctavit, P. (2012). *J. Am. Chem. Soc.* **134**, 222–228.

Bruno, P. & Chappert, C. (1992). *Phys. Rev. B*, **46**, 261–270.

Carbone, C. & Alvarado, S. F. (1987). *Phys. Rev. B*, **36**, 2433–2435.

Carra, P., Thole, B. T., Altarelli, M. & Wang, X. (1993). *Phys. Rev. Lett.* **70**, 694–697.

Chopra, H. D., Yang, D. X., Chen, P. J., Parks, D. C. & Egelhoff, W. F. Jr (2000). *Phys. Rev. B*, **61**, 9642–9652.

Demidov, V. E., Kholin, D. I., Demokritov, S. O., Hillebrands, B., Wegelin, F. & Marien, J. (2004). *Appl. Phys. Lett.* **84**, 2853–2855.

Demokritov, S. O., Bayer, C., Poppe, S., Rickart, M., Fassbender, J., Hillebrands, B., Kholin, D. I., Kreines, N. M. & Liedke, O. M. (2003). *Phys. Rev. Lett.* **90**, 097201.

Demokritov, S., Tsymbal, E., Grünberg, P., Zinn, W. & Schuller, I. K. (1994). *Phys. Rev. B*, **49**, 720–723.

Edwards, D. M., Mathon, J., Muniz, R. B. & Phan, M. S. (1991). *Phys. Rev. Lett.* **67**, 493–496.

Evans, J. & Mosselmans, J. F. W. (1991). *J. Phys. Chem.* **95**, 9673–9676.

Fallarino, L., Sluka, V., Kardasz, B., Pinarbasi, M., Berger, A. & Kent, A. D. (2016). *Appl. Phys. Lett.* **109**, 082401.

Gareev, R. R., Buchmeier, M., Kiessling, M., Woltersdorf, G. & Back, C. H. (2011). *AIP Adv.* **1**, 042155.

Greene, P. K., Osten, J., Lenz, K., Fassbender, J., Jenkins, C., Arenholz, E., Endo, T., Iwata, N. & Liu, K. (2014). *Appl. Phys. Lett.* **105**, 072401.

Grolier, V., Renard, D., Bartenlian, B., Beauvillain, P., Chappert, C., Dupas, C., Ferré, J., Galtier, M., Kolb, E., Mulloy, M., Renard, J. P. & Veillet, P. (1993). *Phys. Rev. Lett.* **71**, 3023–3026.

Grünberg, P., Schreiber, R., Pang, Y., Brodsky, M. B. & Sowers, H. (1986). *Phys. Rev. Lett.* **57**, 2442–2445.

Hathaway, K. B. & Cullen, J. R. (1992). *J. Magn. Magn. Mater.* **104–107**, 1840–1842.

Hellman, F., Hoffmann, A., Tserkovnyak, Y., Beach, G. S. D., Fullerton, E. E., Leighton, Ch., MacDonald, A. H., Ralph, D. C., Arena, D. A., Dürr, H. A., Fischer, P., Grollier, J., Heremans, J. P., Jungwirth, T., Kimel, A. V., Koopmans, B., Krivorotov, I. N., May, S. J., Petford-Long, A. K., Rondinelli, J. M., Samarth, N., Schuller, I. K., Slavin, A. N., Stiles, M. D., Tchernyshyov, O., Thiaville, A. & Zink, B. L. (2017). *Rev. Mod. Phys.* **89**, 025006.

Hellwig, O., Kirk, T. L., Kortright, J. B., Berger, A. & Fullerton, E. E. (2003). *Nat. Mater.* **2**, 112–116.

Hsu, J. H., Tsai, C. L., Lee, C. M. & Saravanan, P. (2015). *J. Appl. Phys.* **117**, 17A715.

Imada, S., Higashiya, A., Okazaki, M., Kashida, M., Sekiyama, A., Taguchi, Y., Iwama, M., Ogusi, K., Tokura, Y. & Suga, S. (2005). *J. Electron Spectrosc. Relat. Phenom.* **144–147**, 711–713.

Jaouen, N., van der Laan, G., Johal, T. K., Wilhelm, F., Rogalev, A., Mylonas, S. & Ortega, L. (2004). *Phys. Rev. B*, **70**, 094417.

Kanchana, V., Vaitheeswaran, G., Alouani, M. & Delin, A. (2007). *Phys. Rev. B*, **75**, 220404R.

Kasuya, T. (1956). *Prog. Theor. Phys.* **16**, 45–57.

Lacroix, C. & Gavigan, J. P. (1991). *J. Magn. Magn. Mater.* **93**, 413–417.

McCord, J., Strache, T., Mönch, I., Mattheis, R. & Fassbender, J. (2011). *Phys. Rev. B*, **83**, 224407.

Ruderman, M. A. & Kittel, C. (1954). *Phys. Rev.* **96**, 99–102.

Saerbeck, T., Loh, N., Lott, D., Toperverg, B. P., Mulders, A. M., Fraile Rodríguez, A., Freeland, J. W., Ali, M., Hickey, B. J., Stampfl, A. P. J., Klose, F. & Stamps, R. L. (2011). *Phys. Rev. Lett.* **107**, 127201.

Sander, D., Valenzuela, S. O., Makarov, D., Marrows, C. H., Fullerton, E. E., Fischer, P., McCord, J., Vavassori, P., Mangin, S., Pirro, P., Hillebrands, B., Kent, A. D., Jungwirth, T., Gutfleisch, O., Kim, C. G. & Berger, A. (2017). *J. Phys. D Appl. Phys.* **50**, 363001.

Schlage, K., Bocklage, L., Erb, D., Comfort, J., Wille, H. C. & Röhlsberger, R. (2016). *Adv. Funct. Mater.* **26**, 7423–7430.

Schrag, B. D., Anguelouch, A., Ingvarsson, S., Xiao, G., Lu, Y., Trouilloud, P. L., Gupta, A., Wanner, R. A., Gallagher, W. J., Rice, P. M. & Parkin, S. S. P. (2000). *Appl. Phys. Lett.* **77**, 2373–2375.

Slonczewski, J. C. (1991). *Phys. Rev. Lett.* **67**, 3172–3175.

Slonczewski, J. C. (1995). *J. Magn. Magn. Mater.* **150**, 13–24.

Stobiecki, F., Urbaniak, M., Szymański, B., Dubowik, J., Kuświk, P., Schmidt, M., Weis, T., Engel, D., Lengemann, D., Ehresmann, A., Sveklo, I. & Maziewski, A. (2008). *Appl. Phys. Lett.* **92**, 012511.

Stöhr, J. (1995). *J. Electron Spectrosc. Relat. Phenom.* **75**, 253–272.

Thakur, P., Cezar, J. C., Brookes, N. B., Choudhary, R. J., Prakash, R., Phase, D. M., Chae, K. H. & Kumar, R. (2009). *Appl. Phys. Lett.* **94**, 062501.

Thole, B. T., Carra, P., Sette, F. & van der Laan, G. (1992). *Phys. Rev. Lett.* **68**, 1943–1946.
Tomaz, M. A., Lin, T., Harp, G. R., Hallin, E., Sham, T. K. & O'Brien, W. L. (1998). *J. Vac. Sci. Technol. A*, **16**, 1359–1363.
Tyer, R., van der Laan, G., Temmerman, W. M., Szotek, Z. & Ebert, H. (2003). *Phys. Rev. B*, **67**, 104409.
Wawro, A., Kurant, Z., Tekielak, M., Jakubowski, M., Pietruczik, A., Böttger, R. & Maziewski, A. (2017*a*). *Appl. Phys. Lett.* **110**, 252405.
Wawro, A., Kurant, Z., Tekielak, M., Nawrocki, P., Milińska, E., Pietruczik, A., Wójcik, M., Mazalski, P., Kanak, J., Ollefs, K., Wilhelm, F., Rogalev, A. & Maziewski, A. (2017*b*). *J. Phys. D Appl. Phys.* **50**, 215004.
Wilhelm, F., Poulopoulos, P., Wende, H., Scherz, A., Baberschke, K., Angelakeris, M., Flevaris, N. K. & Rogalev, A. (2001). *Phys. Rev. Lett.* **87**, 207202.
Yaresko, A. (2016). Private communication.
Yosida, K. (1957). *Phys. Rev.* **106**, 893–898.